OPA1 supports mitochondrial dynamics and immune evasion to CD8$^+$ T cell in lung adenocarcinoma

Ying Wang [1], **Jixiang Wu** [2, 3], **Yadong Li** [4], **Xuanwei Jiang** [5], **Yayun Gu** [5], **Hui Zheng** [1], **Xiaoxuan Wang** [6], **Haotian Zhang** [7], **Yang Cheng** [Corresp. 1]

[1] Geriatric Hospital of Nanjing Medical University, nanjing, china

[2] The Yancheng School of Clinical Medicine of Nanjing Medical University, Yancheng, China

[3] The Sixth Affiliated Hospital of Nantong University, Nanjing, China

[4] the Second Clinical Medical College of Nanjing Medical University, Nanjing, China

[5] Nanjing Medical University, Nanjing, China

[6] Jiangsu Simcere Diagnostics Co., Ltd., Nanjing, China

[7] The first clinical medical college of Nanjing Medical University, Nanjing, China

Corresponding Author: Yang Cheng
Email address: chengyangjsnj@163.com

Background: Mitochondrial fusion and fission were identified to play key roles during multiple biology process. Yet, the genomic mechanism of its activation and the roles in immune evasion in non-small cell lung cancer remains unknown. **Methods:** The transcriptional activation of genes related to mitochondrial dynamics was determined by using multi-omics data in lung adenocarcinoma (LUAD). We elucidated the molecular mechanism and roles of OPA1 promoting lung cancer through single-cell sequence and molecular biological experiments. **Results:** Here, we found that copy number amplification of *OPA1* and *MFN1* were co-occurred and synergistically activated in tumor epithelial cells in lung cancer tissues. Both of *OPA1* and *MFN1* were highly expressed in LUAD tumor tissues and *OPA1* high expression was associated with poor prognosis. In terms of mechanism, the damaged mitochondria released cytochrome c from cristae and activated the apoptotic signaling pathways, inducing cell cycle arrest and cell apoptosis. More interestingly, OPA1 deficiency damaged mitochondrial dynamics and further blocked the respiratory function to increase the sensitivity of tumor epithelial to CD8$^+$ T cells in non-small cell lung cancer . **Conclusions:** Our study demonstrated the high co-occurrence of copy number amplification and co-expression of *OPA1* and *MFN1* in LUAD tissue, and further revealed the contribution of OPA1 in maintaining the mitochondria respiratory function and the ability of immune evasion to CD8$^+$ T cells of LUAD.

OPA1 supports mitochondrial dynamics and immune evasion to CD8$^+$ T cell in lung adenocarcinoma

Ying Wang [1]*, Jixiang Wu [2,3] *, Yadong Li [4]*, Xuanwei Jiang [5], Yayun Gu [5], Hui Zheng [1], Xiaoxuan Wang [6], Haotian Zhang [7], Yang Cheng [1#]

[1] *Center for Health Management, Geriatric Hospital of Nanjing Medical University, Nanjing, China*

[2] *Department of Thoracic and Cardiovascular Surgery, The Yancheng School of Clinical Medicine of Nanjing Medical University, Yancheng, China*

[3] *Department of Thoracic and Cardiovascular Surgery, The Sixth Affiliated Hospital of Nantong University, Yancheng, China*

[4] *Department of Thoracic Surgery, The Second Clinical Medical College of Nanjing Medical University, Nanjing, China*

[5] *State Key Laboratory of Reproductive Medicine, Center for Global Health, School of Public Health, Nanjing Medical University, Nanjing, China*

[6] *State Key Laboratory of Translational Medicine and Innovative Drug Development, Jiangsu Simcere Diagnostics Co., Ltd., Nanjing, China*

[7] *The first clinical medical college of Nanjing Medical University, Nanjing, China*

* These authors contributed equally to this work.

Correspondence

Yang Cheng, Center for Health Management, Geriatric Hospital of Nanjing Medical University, 2 Yi-He Road, Nanjing 210009, China.

Email: chengyangjsnj@163.com

Running head: OPA1 and immune evasion

Abstract

Background: Mitochondrial fusion and fission were identified to play key roles during multiple biology process. Yet, the genomic mechanism of its activation and the roles in immune evasion in non-small cell lung cancer remains unknown.

Methods: The transcriptional activation of genes related to mitochondrial dynamics was determined by using multi-omics data in lung adenocarcinoma (LUAD). We elucidated the molecular mechanism and roles of OPA1 promoting lung cancer through single-cell sequence and molecular biological experiments.

Results: Here, we found that copy number amplification of *OPA1* and *MFN1* were co-occurred and synergistically activated in tumor epithelial cells in lung cancer tissues. Both of *OPA1* and *MFN1* were highly expressed in LUAD tumor tissues and *OPA1* high expression was associated with poor prognosis. In terms of mechanism, the damaged mitochondria released cytochrome c from cristae and activated the apoptotic signaling pathways, inducing cell cycle arrest and cell apoptosis. More interestingly, OPA1 deficiency damaged mitochondrial dynamics and further blocked the respiratory function to increase the sensitivity of tumor epithelial to $CD8^+$ T cells in non-small cell lung cancer.

Conclusions: Our study demonstrated the high co-occurrence of copy number amplification and co-expression of *OPA1* and *MFN1* in LUAD tissue, and further revealed the contribution of OPA1 in maintaining the mitochondria respiratory function and the ability of immune evasion to $CD8^+$ T cells of LUAD.

Keywords: OPA1, lung adenocarcinoma, mitochondrial fusion, immune evasion, $CD8^+$ T cell

Introduction

Lung cancer is the leading deadly malignancy worldwide(Bray et al. 2018), among which non-small cell lung carcinoma (NSCLC) accounts for more than 85% of cases(Wang et al. 2019). Patients diagnosed with NSCLC have an overall 5-year survival rate of less than 18%(Zappa & Mousa 2016).Thus, a deeper exploring of the underlying mechanisms in NSCLC cell progression is crucial for developing effective treatments.

Mitochondria are highly dynamic organelles that are continually undergoing fission and fusion. Emerging evidence has shown that mitochondrial dynamics participates in various cellular activities, including oxidative stress(Yi et al. 2019; Yu et al. 2017; Zhang et al. 2018), apoptosis(Morita et al. 2017; Pena-Blanco & Garcia-Saez 2018; van der Bliek et al. 2013), mitophagy and so on(Chen et al. 2016; van der Bliek et al. 2013; Yoo & Jung 2018). Besides, mitochondrial dynamics play a pivotal role in mitochondrial dysfunction, which is closely related to tumorigenesis and tumor progression(Simula et al. 2017). Mitochondrial fusion is driven by mitofusin 1 and 2 (MFN1/2) and optic atrophy 1 (OPA1) and mitochondrial fission is driven by dynamin 1 like (DNM1L) (Westermann 2010). Recently, studies have demonstrated that dysregulated expression of mitochondrial dynamic proteins such as DNM1L and MFN1/2 in lung, colon and breast cancer (Zhang et al. 2020; Zou et al. 2016) is important for cell cycle progression(Rehman et al. 2012). However, the mechanism of the related gene expression activation and their roles in LUAD remains unknown.

The inflammatory cell infiltrates formed in human cancers could promote natural disease progression or, conversely, contribute to antitumor effects(van der Leun et al. 2020). It is well documented that CD8+ T cells have the ability to recognize and eliminate cancer cells(van der Leun et al. 2020). Here, we found that copy number amplification of *OPA1* and *MFN1* were co-occurred and synergistically activated in lung cancer tissues. Moreover, activation of OPA1 promoted mitochondrial dynamics in tumor epithelial cells to escape CD8+ T cells killing.

Materials and methods

Immunohistochemistry analysis

All of the tissues were handled with the following steps: 1) Deparaffinizing and rehydrating the paraffin section; 2) Antigen retrieval; 3) For cooling to room temperature before proceeding, the sections were placed in PBS (pH=7.4) and shaken on a decolorization shaker 3 times for 5 minutes each; 4) Blocking endogenous peroxidase activity; 5) Primary antibody incubation and secondary antibody incubation; 6) DAB chromogenic reaction nuclear counterstaining, Dehydration and mounting. Finally, staining of the tissues were visualized with a microscope, and images were acquired and analyzed. H-score: The depth and quantity of positivity was scored by Quant Center -an analysis software matched with a 3D scanner, which can only quantify the brown–yellow color of DAB. The larger the value, the stronger is the positivity. The assay refers to the methods in previously reported research(Yin et al. 2021).

ATP Assays

ATP was analized by enhanced ATP assay kit (Beyotime, S0027). The assay were performed ref to the protocols reported by previous studies(Kuang et al. 2021).

Protein isolation, Western blotting and antibodies

Total proteins were collected from treated cell lines with RIPA buffer containing protease inhibitors: phenylmethanesulfonyl fluoride (PMSF, Beyotime, Haimen, China) and cocktail (MedChemExpress, Shanghai, China). The BCA method was used to measure protein concentrations. Western blotting was performed as previously described(Xie et al. 2018). The antibodies used were as follows: anti-OPA1 (1:1000, Abcam, ab157457); anti-cytochrome C (1:5000, Abcam, ab133504); and anti-GAPDH (1:1000, Beyotime, AG019).

Cell culture and transfection

Human LUAD cell lines (NCI-H1299 and NCI-A549) were obtained from the Shanghai Institute of Biochemistry and Cell Biology and have been independently validated by STR DNA fingerprinting at Shanghai Zhong Qiao Xin Zhou Biotechnology (Shanghai, China). Cells were cultured in DMEM (Gibco, Carlsbad, MA) supplemented with 10% fetal bovine serum (Gibco, Carlsbad, MA). These cells were grown at 37 °C with 5% CO_2 in a humidified incubator.

The shRNAs specific for *OPA1* were synthesized (RiboBio, Guangzhou, China), and the overexpression plasmid targeting *OPA1* was custom-designed (GENOME, Nanjing, China). The plasmid DNA or shRNA was transiently transfected into cells with Lipofectamine 2000 reagent (Invitrogen, Shanghai, China).

Cell proliferation assay

Cell proliferation was analyzed by CCK8 (Dojindo, Japan) and colony formation assays per the manufacturer's instructions. A total of 4×10^3 cells were seeded in 96-well plates (Corning, New York, USA), and the culture medium was replaced with 10 μl CCK8 solution mixed with 100 μl RPMI 1640 or DMEM every 24 hours and then incubated at 37 °C. The optical density value was measured using a TECAN Infinite M200 Multimode microplate reader (450nm, Tecan, Mechelen, Belgium). Values were obtained from 5 technical replicates. A total of 1×10^3 cells were seeded in 6-well plates (Corning, New York, USA) and maintained for 14 days. Cell colonies were fixed with methanol and then stained with crystal violet (Beyotime, Haimen, China) for 30 min. All wells were photographed and counted. Each assay was performed at least three times.

Transwell assays

The migration and invasion capacity of lung cancer cells were investigated using Transwell plates (Corning Sparks, MD). Culture medium containing 10% FBS was added to the bottom compartment of the chamber as a chemoattractant. A total of 2×10^4 cells/100 μl of lung cancer cells were plated on the upper chambers in serum-free medium and cultured for 24 h for migration and 36 h for invasion. Cells that adhered to the bottom of the membrane were then fixed with methanol for 15 min, stained with crystal violet (Beyotime, Haimen, China), and quantified from five averaged fields via a Q-fired cooled CCD camera attached to an Olympus microscope. The assay was repeated three times in duplicate.

Seahorse Assay

Glycolysis and mitochondrial metabolism assessments were performed using NCI-H1299 cells, which were seeded at an optimized cell density of 40,000 (NCI-H1299) cells/well. One day later, the cells were incubated for 24 h with vehicle Gibco DMEM. Then the evaluation of mitochondrial ATP production, spare respiratory capacity and proton leak were analized as the protocols reported by previously studies(Kuang et al. 2021).

Metabolomics Analysis

$1*10^7$ cells in different groups were seeded in 75 culture dishes and treated with different concentrations of NCI-H1299 (0, 2.5, 5, and 10 μ M). Then the cells were harvested and kept in liquid nitrogen. The metabolites were extracted and subjected to analysis of central carbon metabolism(Zhang et al. 2021).

Analysis of cell cycle progression and apoptosis using flow cytometry

Cells were harvested using 0.25% trypsin and washed with PBS. After resuspending in PBS and counting, 2×10^5 cells were centrifuged and supernatant. Annexin V-FITC and propidium iodide (PI) staining solution were added with low-speed shaking and keep in the dark for 10 min.

Then the cells were resuspended in cold 70% ethanol and 4°C overnight. Samples were centrifuged and washed with PBS. 150 μl RNase A and PI staining solution were then added to each tube and were then incubated at 4°C. 20 min later, the samples were analyzed using flow cytometry and the ratio of cell among the G1, S and G2/M phases were analyzed(Zuo et al. 2014).

RNA preparation and quantitative real-time RT-PCR (qRT-PCR)

Total RNA was extracted by using TRIzol reagent (Invitrogen; Thermo Fisher Scientific, Inc., Waltham, MA, USA). Approximately 1000 ng of RNA was used for the reverse transcription reaction.

The cDNA was amplified on a QuantStudio™ 7 Flex Real-Time PCR System in triplicate. Analyses of relative gene expression were determined using the $2^{-\Delta Ct}$ method with GAPDH as the internal reference gene. The primers used are listed in Supplementary Table 1.

RNA sequencing and analysis

OPA1 knockdown and control LUAD cells was conducted using RNA sequencing (RNA-seq) as described previously(Wang et al. 2018). The RNA concentration and quality of each sample were assessed. mRNA was purified from total RNA using oligo (dT) beads to obtain the mRNA-seq library according to a stranded protocol (Illumina, San Diego, USA) and then sequenced using an Illumina HiSeq X Ten system. The statistical power of this experimental design, was calculated in Source Package RNASeqPower in R (version "4.2") with the calculated power of 0.89. Three biological replicates were involved in both of the two groups for the RNA-seq analysis. 6G, 294x depth raw data per sample were filtered and processed by Q30 and aligned to the mouse reference genome GRCh37/Gencode v19 with STAR software (v2.5.3a). Then, assembly and quantification of the transcripts were accomplished with RESM software (Version 1.3.3) guided by the Ensembl gtf gene

annotation file (http://www.ensembl.rog/). Read counts were used for the measurements of the relative abundance of the transcripts. The differential expression genes (DEG) was identifying using the limma packages in with an adjusted P value <0.05 and |log2[fold change (FC)]| >0.5. We further conducted an enrichment analysis of the DEGs with DAVID Bioinformatics Resources (version 6.8;https://david.ncifcrf.gov/). The top 10 GO terms of the biological processes were examined. GSEA was performed using the R package cluster Profiler as previously reported(Chen et al. 2020).

Acquisition and processing of TCGA database

Transcriptome RNA-seq data of 1111 NSCLC samples (LUAD, normal: 59 cases; tumor: 513 cases) and lung squamous cell carcinoma samples (LUSC, normal: 50 cases; tumor: 489 cases) were obtained from the TCGA database (https://portal.gdc.cancer.gov/) with level 3. The association between OPA1 and MFN1 expression and survival in all tumor tissue samples was analyzed by Cox regression, which was obtained from http://www.oncolnc.org/cancer/.

Single-cell RNA sequencing (scRNA-seq) statistical analysis

The 10x Genomics scRNA-seq matrix of early stage LUAD tumor from primary lung tissues (tLUNG) were obtained from the previous study(Kim et al. 2020). The filtered and batched digital gene expression matrix (UMI counts per gene per cell) of 11 LUAD tLUNG samples was imported in R version 4.1 using Seurat v4.1.0. In our study, we used the t-Distributed Stochastic Neighbor Embedding (tSNE) algorithm for visual processing of this dimension-reduced dataset. Besides, main cell types were identified by scoring canonical cell type markers across clusters(Bischoff et al. 2021).

To score the cell cycle phases of each single cell, we used the Cell Cycle Scoring function in Seurat. This function calculated the cell cycle score based on previously published canonical marker genes(Nestorowa et al. 2016). To analysis cell-cell chat we applied the Cell Chat R package v1.4.0 and used the Cell Chat website https://github.com/sqjin/CellChat.

Statistical analysis

We provided our raw numeric data for review and publication so the statistical analysis performed in our study can be checked (as shown in Supplemental Table 2-5). All statistical analyses were performed by using R software. For experimental data, the Student's t test or one-way ANOVA was used to assess differences in

treatment groups using GraphPad Prism software (version 6.01). The results are expressed as the mean ± s.e.m. of three independent experiments. The significance threshold was set as a *P* value <0.05.

Results

Molecular mechanism underlying the mitochondria dynamics in NSCLC

To systematically evaluate the mechanism of mitochondria dynamics in NSCLC development, we performed the differential expression analysis of the four classical mitochondrial dynamics-related genes between the normal and tumor samples in the TCGA database (Figure. 1A). We identified 3 differential genes ($p < 0.05$), which were significantly up-regulated in the tumor samples, including *OPA1, MFN1* and *DNM1L*. To further explore the mechanism of their transcriptional activation, we used a combined analysis with genomic data and found *OPA1* and *MFN1* have higher genomic alteration rate of 17% and 20%, with copy number variation (CNV) as the most common mutation type (Figure. 1B). The alteration type of the two genes is shown in Figure. 1C, mainly consisting of gain and amplification. Further analysis found the significant correlation of genomic amplification and gene expression of both *OPA1* and *MFN1* (Figure. 1D). It is worth noting that NSCLC patients with OPA1 and MFN1 gain or amplification tended to have co-occurrence implying their synergistic roles in mitochondrial dynamics. Immunohistochemical (IHC) results also revealed that the protein expression of OPA1 was significantly increased in LUAD tumor tissues (Figure. 1E). In addition, Kaplan–Meier curves revealed that higher expression of *OPA1* was significantly correlated with poor survival in LUAD patients (Figure. 1F).

Loss of OPA1 induced mitochondrial dysfunction and metabolic reprogramming

We further examined transcriptional datasets from sh*OPA1* and control cells, and the PCA is shown in Figure. S1A. With a filter *P* value < 0.05 and |log2Fold-change|> 1, significantly different genes consisting of 2261 down-regulated genes and 3500 up-regulated genes in LUAD are shown in a volcano plot (Figure. 2A). Clustering analysis is shown in the heatmap in Figure. 2B. Specifically, we performed a GO analysis of these genes and revealed that they were involved in many signaling pathways, including mitochondrial function, ATP binding, ATP-dependent DNA helicase activity and membrane pathways (Figure. 2C), which provided clues about mitochondria. KEGG & COG_ONTOLOGY analysis also revealed dysfunction of mitochondrial metabolism (Figure. S1B&C). Furthermore, GSEA was performed to verify that the function of mitochondria

and ATP production were inhibited in Sh*OPA1* cells (Figure. 2D&E). Then, we conducted electron microscopy, and the results showed that the loss of OPA1 caused a decreased number of mitochondria and an abnormal mitochondrial morphology, especially presenting a disordered arrangement of cristae and swelling (Figure. 2F). Mitochondria are the main organelles that produce ATP, so we measured ATP production. ATP production was significantly decreased in Sh*OPA1* cells, further indicating disorder of mitochondria with the loss of OPA1 (Figure. 2G).

OPA1 modulates the TCA metabolic process in LUAD cells

The mitochondrial metabolism of central carbon metabolism and oxygen consumption were further measured in NCI-H1299 cell lines. The obtained score plot of PCA analysis enabled a clear separation between the control group and the sh*OPA1* group (Figure. 3A). In addition, we identified 49 differentially abundant metabolites, consisting of 30 down-regulated and 19 up-regulated metabolites, based on a volcano plot (Figure. S1D). Variable importance in projection showed that significantly different metabolites were mainly involved in the processes of TCA and glycolysis (Figure. 3B). The relationship between the samples and metabolites is shown in Figure. S1E. When these significantly altered metabolites were subjected to unsupervised hierarchical clustering, a more defined pattern of metabolic alterations induced by exercise was observed. The results revealed significant alterations in nucleotide and amino acid metabolism, glycolysis, and the TCA cycle (Figure. 3C-D). A heatmap of all the metabolites is shown in Fig. S1F. In addition, the oxygen consumption rate (OCR) was significantly lower in sh*OPA1* than in control cells, and proton leakage and ATP production were decreased (Figure. 3E&F). The above results demonstrated that the loss of OPA1 blocked the activity of mitochondria to balance metabolism.

OPA1$^+$ tumor epithelial cells decreased its immune response to CD8$^+$ T cell

To further explore the roles of OPA1 in tumorigenesis, we performed RNA-seq analysis and identified increased activity of immune response pathways (pathway of “immune response” and “MHC class II protein complex binding”) in OPA1 knocked down LUAD cells. GSEA analysis show the higher activity of immune response and the mRNA expression of related gene, B2M, GBP2, CD24, HLA-F, CTSS, all increased in OPA1 knocked

down LUAD cells. Moreover, we used single cell sequencing data to further analysis the immune response of $OPA1^+$ tumor epithelial cell to immune cells. All cells were divided into 19 clusters according to the t-SNE clustering algorithm and exhibited a higher expression of *OPA1* in tumor epithelial cell (Figures 4A-B). Also, the proportion of OPA1 and MFN1 in various cells tend to be more distributed in tumor epithelial cells. Interestingly, it was found that OPA1 and MFN1 were strongly correlated in tumor epithelial cells (Figure 4C). We further performed a GO analysis of the significantly different genes in $OPA1^+$ and $OPA1^-$ patients in different cell types (Figure. 4D). MKi67 expression is found within proliferating cells alone under general conditions and we found that MKi67 was higher expressed in $OPA1^+$ cells (Figure. 4E). Go analysis of up-regulated and down-regulated genes showed that up-regulated genes mainly played a role in cell adhesion, while down-regulated genes mainly concentrated in immune response-related pathways (Figure. 4F-G). By comparing the interaction network between $OPA1^+$ and $OPA1^-$ tumor tissues, we found that the communication of tumor epithelial with $CD8^+$ T cells was significantly increased in $OPA1^-$ tumor tissues (Figure. 4H). This suggests that $OPA1^-$ tumor epithelial cells may regulate the immune responses strongly, while $OPA1^+$ tumor epithelial cells are associated with immune escape (Figure. 4H).

OPA1 deficiency induced cell death via mitochondrial stress

Having confirmed the decreased activity of mitochondria, we further measured mitochondrial membrane potential. Mitochondrial membrane potential is a key mediator responsible for the activity of mitochondria(Zorov et al. 2006). As shown in Figure. 5A&B, the loss of OPA1 caused a lower mitochondrial membrane potential, characterized by red fluorescence (TMRM). With the damaged mitochondrial membrane potential, cytochrome c was released into the cytosol (Figure. 5C). Cytochrome c is critical in the activation of programmed cell death pathway.(Ow et al. 2008) Therefore, we detected apoptosis by Annexin V-FITC in NCI-H1299 cells. The results showed more apoptotic cells with the loss of OPA1 (Figure. 5F). In addition, we detected the influence on the cell cycle of the damaged mitochondria. Flow cytometric analysis and RT-PCR verified that the cell cycle was blocked in G1 phase (Figure. 5D&E), accelerating the process of apoptosis.

OPA1 modulates enhanced proliferation and migration of LUAD cell lines

To evaluate the roles of OPA1 in LUAD, we knocked down *OPA1* through virus infection (shRNAs) in the NCI-A549 cell line (Figure. 6A). We found that low OPA1 expression significantly reduced the cell growth rate (Figure. 6B) and resulted in fewer colonies (Figure. 6C). Moreover, transwell assays showed that knockdown of *OPA1* inhibited cell migration compared with the negative control (Figure. 6D). Similarly, inhibition of cell growth, cloning and migration were observed in sh*OPA1* NCI-H1299 cells (Figure. 6E-H). In addition, we overexpressed *OPA1* in NCI-A549 cells (Figure. 6I), which significantly increased the cell growth rate (Figure. 6J) and colony numbers (Figure. 6K). Additionally, transwell assays showed that OPA1 accelerated the speed of cell migration compared with the negative control (Figure. 6L). These findings suggested the essential role of OPA1 in regulating the progression of LUAD.

Discussion

Although studies have indicated that OPA1 is a key gene involved in the process of mitochondrial fusion, the loss of which will block the process of metabolism in tumor cells(Li et al. 2020), the underlying mechanism remains poorly defined, and the detailed function of OPA1 in LUAD development remains unknown. In this study, we revealed that knockdown of *OPA1* failed to maintain a balance of mitochondrial dynamics and further enhanced the sensitivity of tumor epithelial cells to immune cells.

CNVs are regions of the genome that vary in integer copy number. CNVs, which comprise both amplifications and deletions of DNA sequences, have been identified across all domains of life. Studies demonstrated that the frequency of CNVs determined genetic diversity, which is an important source of heritable and somatic human diseases(Lauer & Gresham 2019). As shown in the TCGA database, *OPA1* is highly expressed in LUAD tissues, and the copy number amplification of *OPA1* was strongly and positively correlated with its mRNA expression. Therefore, we inferred that CNV in OPA1 correlates with LUAD susceptibility.

Metabolic reprogramming is a typical characteristic in tumor cells(Sun et al. 2018). And mitochondria are just key centers to control bioenergetics and metabolism(Annesley & Fisher 2019). The morphodynamics of mitochondria, comprising fusion and fission processes, are closely associated with mitochondrial functions and are often dysregulated in cancer(Zong et al. 2016). OPA1 is a critical gene involved in mitochondrial fusion(Del Dotto et al. 2018). We identified that it has a high occurrence rate of copy number variation and is highly expressed in LUAD tissues based on public databases and immunohistochemical results. OPA1 regulates mitochondrial dynamics; it is located at the inner mitochondrial membrane and is the key factor for maintaining mitochondrial fusion and preserving cellular health(Wai et al. 2015). OPA1 governs the delicate balance between fission and fusion of mitochondrial. A impaired balance caused mitochondrial fragmentation and ultimately resulted in cell apoptosis and were usually observed under stress or pathologic conditions(MacVicar & Langer 2016). Our electron microscopy results indicated that the loss of OPA1 resulted in a disordered number and morphology of mitochondria. Mitochondria showed a decrease in number and fragmentation.

The use of $CD8^+$ T cells, with the ability to detect and eradicate cancer cells has been a focus of clinical cancer therapy for over 20 years. Tumors express specific neo antigens1-6 and self-antigens, and CD8+ T cells reactive against such antigens were identified in tumors. In our study, the disturbed mitochondrial dynamics

attributed to the loss of OPA1 caused the inhibition of TCA and the mitochondrial respiratory chain, finally significantly decreasing the production of ATP in LUAD. Our present work further reveals that knockdown of OPA1 mediated high expression of immune response related genes contributes to the cell-cell communication of tumor epithelial and T cells. Thus, a metabolic reprogramming-associated immune-activated status in the tumor cells holds a latent value in predicting tumor response to immunotherapy and in inventing new metabolic targets in the combined immunotherapy with radiation or chemotherapy. However, more studies were needed to deeply explore the mechanism of how mitochondria dynamics mediated metabolic reprogramming to active immune response of epithelia cells to immune cells.

In addition to the dysfunction of metabolism, studies have also verified that the loss of OPA1 causes the disorder of fusion in the mitochondrial inner membrane, then cytochrome c release from the cristae and activate the pathway of apoptosis(Kalpage et al. 2020). Our data demonstrated that knockdown of OPA1 disrupted the mitochondrial membrane potential and accelerated cytochrome c release from cristae. The apoptotic pathway was activated by cytochrome c acceleration of the process of apoptosis. In addition, inhibition of the cell cycle caused by the failure of metabolism jointly led to apoptosis.

Conclusions

In summary, our results showed that the process of mitochondrial fusion caused by OPA1 was activated in LUAD, which enhanced mitochondrial metabolism to fuel tumor growth and inhibited cell apoptotic pathways (Figure. 7). These findings suggest potential mitochondria-targeted therapy and more effective treatment modalities.

Funding: This work was supported by grants 81903385 and 81902836 from the National Natural Science Foundation of China.

Institutional Review Board Statement: The study was conducted according to the guidelines of Geriatric Hospital of Nanjing Medical University.

Informed Consent Statement: Informed consent was obtained from all subjects involved in the study.

Conflicts of Interest: No potential conflicts of interest relevant to this article were reported. Xiaoxuan Wang participated in the collation of some data and pictures in our study, who employed by Jiangsu Simcere Diagnostics Co., Ltd., and also declared there are no competing interests.

References

Annesley SJ, and Fisher PR. 2019. Mitochondria in Health and Disease. *Cells* **7(8)** 10.3390/cells8070680

Bischoff P, Trinks A, Obermayer B, Pett JP, Wiederspahn J, Uhlitz F, Liang X, Lehmann A, Jurmeister P, Elsner A, Dziodzio T, Ruckert JC, Neudecker J, Falk C, Beule D, Sers C, Morkel M, Horst D, Bluthgen N, and Klauschen F. 2021. Single-cell RNA sequencing reveals distinct tumor microenvironmental patterns in lung adenocarcinoma. *Oncogene* **50(40)**:6748-6758 10.1038/s41388-021-02054-3

Bray F, Ferlay J, Soerjomataram I, Siegel RL, Torre LA, and Jemal A. 2018. Global cancer statistics 2018: GLOBOCAN estimates of incidence and mortality worldwide for 36 cancers in 185 countries. *CA Cancer J Clin* **6(68)**:394-424 10.3322/caac.21492

Chen M, Chen Z, Wang Y, Tan Z, Zhu C, Li Y, Han Z, Chen L, Gao R, Liu L, and Chen Q. 2016. Mitophagy receptor FUNDC1 regulates mitochondrial dynamics and mitophagy. *Autophagy* **4(12)**:689-702 10.1080/15548627.2016.1151580

Chen Q, Lei JH, Bao J, Wang H, Hao W, Li L, Peng C, Masuda T, Miao K, Xu J, Xu X, and Deng CX. 2020. BRCA1 Deficiency Impairs Mitophagy and Promotes Inflammasome Activation and Mammary Tumor Metastasis. *Adv Sci (Weinh)* **6(7)**:1903616 10.1002/advs.201903616

Del Dotto V, Fogazza M, Lenaers G, Rugolo M, Carelli V, and Zanna C. 2018. OPA1: How much do we know to approach therapy? *Pharmacol Res***131)**:199-210 10.1016/j.phrs.2018.02.018

Kalpage HA, Wan J, Morse PT, Zurek MP, Turner AA, Khobeir A, Yazdi N, Hakim L, Liu J, Vaishnav A, Sanderson TH, Recanati MA, Grossman LI, Lee I, Edwards BFP, and Huttemann M. 2020. Cytochrome c phosphorylation: Control of mitochondrial electron transport chain flux and apoptosis. *Int J Biochem Cell Biol***121)**:105704 10.1016/j.biocel.2020.105704

Kim N, Kim HK, Lee K, Hong Y, Cho JH, Choi JW, Lee JI, Suh YL, Ku BM, Eum HH, Choi S, Choi YL, Joung JG, Park WY, Jung HA, Sun JM, Lee SH, Ahn JS, Park K, Ahn MJ, and Lee HO. 2020. Single-cell RNA sequencing demonstrates the molecular and cellular reprogramming of metastatic lung adenocarcinoma. *Nat Commun* **1(11)**:2285 10.1038/s41467-020-16164-1

Kuang W, Zhang J, Lan Z, Deepak R, Liu C, Ma Z, Cheng L, Zhao X, Meng X, Wang W, Wang X, Xu L, Jiao Y, Luo Q, Meng Z, Kee K, Liu X, Deng H, Li W, Fan H, and Chen L. 2021. SLC22A14 is a mitochondrial riboflavin transporter required for sperm oxidative phosphorylation and male fertility. *Cell Rep* **3(35)**:109025 10.1016/j.celrep.2021.109025

359 **Lauer S, and Gresham D. 2019.** An evolving view of copy number variants. *Curr Genet* **6(65)**:1287-
360 1295 10.1007/s00294-019-00980-0
361 **Li M, Wang L, Wang Y, Zhang S, Zhou G, Lieshout R, Ma B, Liu J, Qu C, Verstegen MMA,**
362 **Sprengers D, Kwekkeboom J, van der Laan LJW, Cao W, Peppelenbosch MP, and Pan Q.**
363 **2020.** Mitochondrial Fusion Via OPA1 and MFN1 Supports Liver Tumor Cell Metabolism and
364 Growth. *Cells* **1(9)** 10.3390/cells9010121
365 **MacVicar T, and Langer T. 2016.** OPA1 processing in cell death and disease - the long and short of it.
366 *Journal of cell science* **12(129)**:2297-2306 10.1242/jcs.159186
367 **Morita M, Prudent J, Basu K, Goyon V, Katsumura S, Hulea L, Pearl D, Siddiqui N, Strack S,**
368 **McGuirk S, St-Pierre J, Larsson O, Topisirovic I, Vali H, McBride HM, Bergeron JJ, and**
369 **Sonenberg N. 2017.** mTOR Controls Mitochondrial Dynamics and Cell Survival via MTFP1. *Mol*
370 *Cell* **6(67)**:922-935 e925 10.1016/j.molcel.2017.08.013
371 **Nestorowa S, Hamey FK, Pijuan Sala B, Diamanti E, Shepherd M, Laurenti E, Wilson NK, Kent**
372 **DG, and Gottgens B. 2016.** A single-cell resolution map of mouse hematopoietic stem and
373 progenitor cell differentiation. *Blood* **8(128)**:e20-31 10.1182/blood-2016-05-716480
374 **Ow Y-LP, Green DR, Hao Z, and Mak TW. 2008.** Cytochrome c: functions beyond respiration. *Nature*
375 *reviews Molecular cell biology* **7(9)**:532-542 10.1038/nrm2434
376 **Pena-Blanco A, and Garcia-Saez AJ. 2018.** Bax, Bak and beyond - mitochondrial performance in
377 apoptosis. *FEBS J* **3(285)**:416-431 10.1111/febs.14186
378 **Rehman J, Zhang HJ, Toth PT, Zhang Y, Marsboom G, Hong Z, Salgia R, Husain AN, Wietholt C,**
379 **and Archer SL. 2012.** Inhibition of mitochondrial fission prevents cell cycle progression in lung
380 cancer. *FASEB J* **5(26)**:2175-2186 10.1096/fj.11-196543
381 **Simula L, Nazio F, and Campello S. 2017.** The mitochondrial dynamics in cancer and immune-
382 surveillance. *Semin Cancer Biol***47)**:29-42 10.1016/j.semcancer.2017.06.007
383 **Sun L, Suo C, Li ST, Zhang H, and Gao P. 2018.** Metabolic reprogramming for cancer cells and their
384 microenvironment: Beyond the Warburg Effect. *Biochim Biophys Acta Rev Cancer* **1(1870)**:51-66
385 10.1016/j.bbcan.2018.06.005
386 **van der Bliek AM, Shen Q, and Kawajiri S. 2013.** Mechanisms of mitochondrial fission and fusion.
387 *Cold Spring Harb Perspect Biol* **6(5)** 10.1101/cshperspect.a011072
388 **van der Leun AM, Thommen DS, and Schumacher TN. 2020.** CD8(+) T cell states in human cancer:
389 insights from single-cell analysis. *Nat Rev Cancer* **4(20)**:218-232 10.1038/s41568-019-0235-4
390 **Wai T, Garcia-Prieto J, Baker MJ, Merkwirth C, Benit P, Rustin P, Ruperez FJ, Barbas C, Ibanez**
391 **B, and Langer T. 2015.** Imbalanced OPA1 processing and mitochondrial fragmentation cause heart
392 failure in mice. *Science (New York, NY)* **6265(350)**:aad0116 10.1126/science.aad0116
393 **Wang C, Yin R, Dai J, Gu Y, Cui S, Ma H, Zhang Z, Huang J, Qin N, Jiang T, Geng L, Zhu M, Pu**
394 **Z, Du F, Wang Y, Yang J, Chen L, Wang Q, Jiang Y, Dong L, Yao Y, Jin G, Hu Z, Jiang L,**
395 **Xu L, and Shen H. 2018.** Whole-genome sequencing reveals genomic signatures associated with
396 the inflammatory microenvironments in Chinese NSCLC patients. *Nature communications*
397 **1(9)**:2054 10.1038/s41467-018-04492-2
398 **Wang L, Zhao D, Qin K, Rehman FU, and Zhang X. 2019.** Effect and biomarker of Nivolumab for
399 non-small-cell lung cancer. *Biomed Pharmacother***117)**:109199 10.1016/j.biopha.2019.109199

Westermann B. 2010. Mitochondrial fusion and fission in cell life and death. *Nat Rev Mol Cell Biol* **12(11)**:872-884 10.1038/nrm3013

Xie K, Zhang K, Kong J, Wang C, Gu Y, Liang C, Jiang T, Qin N, Liu J, Guo X, Huo R, Liu M, Ma H, Dai J, and Hu Z. 2018. Cancer-testis gene PIWIL1 promotes cell proliferation, migration, and invasion in lung adenocarcinoma. *Cancer Med* **1(7)**:157-166 10.1002/cam4.1248

Yi X, Guo W, Shi Q, Yang Y, Zhang W, Chen X, Kang P, Chen J, Cui T, Ma J, Wang H, Guo S, Chang Y, Liu L, Jian Z, Wang L, Xiao Q, Li S, Gao T, and Li C. 2019. SIRT3-Dependent Mitochondrial Dynamics Remodeling Contributes to Oxidative Stress-Induced Melanocyte Degeneration in Vitiligo. *Theranostics* **6(9)**:1614-1633 10.7150/thno.30398

Yin D, Ling S, Wang D, Dai Y, Jiang H, Zhou X, Paludan SR, Hong J, and Cai Y. 2021. Targeting herpes simplex virus with CRISPR-Cas9 cures herpetic stromal keratitis in mice. *Nat Biotechnol* **5(39)**:567-577 10.1038/s41587-020-00781-8

Yoo SM, and Jung YK. 2018. A Molecular Approach to Mitophagy and Mitochondrial Dynamics. *Mol Cells* **1(41)**:18-26 10.14348/molcells.2018.2277

Yu Y, Wang L, Delguste F, Durand A, Guilbaud A, Rousselin C, Schmidt AM, Tessier F, Boulanger E, and Neviere R. 2017. Advanced glycation end products receptor RAGE controls myocardial dysfunction and oxidative stress in high-fat fed mice by sustaining mitochondrial dynamics and autophagy-lysosome pathway. *Free Radic Biol Med***112)**:397-410 10.1016/j.freeradbiomed.2017.08.012

Zappa C, and Mousa SA. 2016. Non-small cell lung cancer: current treatment and future advances. *Transl Lung Cancer Res* **3(5)**:288-300 10.21037/tlcr.2016.06.07

Zhang C, Liu T, Luo P, Gao L, Liao X, Ma L, Jiang Z, Liu D, Yang Z, Jiang Q, Wang Y, Tan X, Luo S, Wang Y, and Shi C. 2021. Near-infrared oxidative phosphorylation inhibitor integrates acute myeloid leukemia-targeted imaging and therapy. *Sci Adv* **1(7)** 10.1126/sciadv.abb6104

Zhang T, Wu P, Zhang JH, Li Y, Xu S, Wang C, Wang L, Zhang G, Dai J, Zhu S, Liu Y, Liu B, Reis C, and Shi H. 2018. Docosahexaenoic Acid Alleviates Oxidative Stress-Based Apoptosis Via Improving Mitochondrial Dynamics in Early Brain Injury After Subarachnoid Hemorrhage. *Cell Mol Neurobiol* **7(38)**:1413-1423 10.1007/s10571-018-0608-3

Zhang Z, Li TE, Chen M, Xu D, Zhu Y, Hu BY, Lin ZF, Pan JJ, Wang X, Wu C, Zheng Y, Lu L, Jia HL, Gao S, Dong QZ, and Qin LX. 2020. MFN1-dependent alteration of mitochondrial dynamics drives hepatocellular carcinoma metastasis by glucose metabolic reprogramming. *Br J Cancer* **2(122)**:209-220 10.1038/s41416-019-0658-4

Zong W-X, Rabinowitz JD, and White E. 2016. Mitochondria and Cancer. *Molecular cell* **5(61)**:667-676 10.1016/j.molcel.2016.02.011

Zorov DB, Juhaszova M, and Sollott SJ. 2006. Mitochondrial ROS-induced ROS-release: An update and review. *Biochimica Et Biophysica Acta-Bioenergetics*:52-53

Zou P, Liu L, Zheng LD, Payne KK, Manjili MH, Idowu MO, Zhang J, Schmelz EM, and Cheng Z. 2016. Coordinated Upregulation of Mitochondrial Biogenesis and Autophagy in Breast Cancer Cells: The Role of Dynamin Related Protein-1 and Implication for Breast Cancer Treatment. *Oxid Med Cell Longev***2016)**:4085727 10.1155/2016/4085727

Zuo X, Qin Y, Zhang X, Ning Q, Shao S, Luo M, Yuan N, Huang S, and Zhao X. 2014. Breast cancer cells are arrested at different phases of the cell cycle following the re-expression of ARHI. *Oncol Rep* **5(31)**:2358-2364 10.3892/or.2014.3107

Figure legends

Figure 1. The high expression and function of *OPA1* in LUAD.

(A) Mitochondrial dynamics-related genes (*MFN1/2*, *OPA1* and *DNM1L*) are highly expressed in tumor tissues based on TCGA database. (B) Schematic diagram showing somatic alterations in the genes identified in NSCLC. Amplification (red) was displayed. (C-D) Copy number alterations of OPA1 and MFN1 in NSCLC samples from TCGA data (C) and a box plot showing the association between mRNA levels and gene amplification or deletion (D). (E) Immunohistochemical examination of OPA1 expression in adjacent (N=55) and tumor (N=55) tissues, H-score: the depth and quantity of positivity scored by Quant Center, an analysis software matching with 3D scanner. H-score detected by image j and used to evaluate the protein expression of OPA1. (F) The correlation between the expression of OPA1, MFN1 and survival of LUAD patients. For D to F, data are expressed as the means ± SEM. The statistical analysis was carried out using t-test.

Figure 2. Loss of *OPA1* induced mitochondrial dysfunction and decreased ATP production.

(A) Volcano plot of statistical significance (P<0.05) against fold change (ratio of Sh*OPA1*/Control group), demonstrating the most significantly differentially expressed genes by genome-wide transcriptomic analysis between Control and Sh*OPA1* NCI-H1299 cells. (B) Heat map of color-coded expression levels of differentially expressed genes (two-way ANOVA (n=3)). (C) GO pathway enrichment analysis within the complete set of differentially expressed genes. (D, E) GSEA enrichment plots showing that loss of *OPA1* results in the dysfunction of MITOCHONDRIA_GENE_MODULE and ATP_METABOLIC_PROCESS gene set. (F) Transmission electron microscopy was used to observe mitochondrial morphology and combined with Image J measurement to analyze the changes in the area and number in Control and Sh*OPA1* NCI-H1299 cells. Scale bars, 500nm. (G) ATP production was detected in Control and Sh*OPA1* cells. Abbreviations: CC, Cellular Component; BP, Biological Process; MF, Molecular Function. For F to G, the bars represent mean ± SEM. The statistical analysis was carried out using t-test, NS denotes no significant, ** denotes $P < 0.01$.

Figure 3. Knockdown of *OPA1* decreased the metabolic efficiency in NCI-H1299 cells.

(A) Metabolites were analyzed by PLS-DA. Each principal component is labeled with the corresponding percent values. (B) Variable importance on projection (VIP) represented the importance of the substance in the PLS-DA model. (C) Heatmap analysis of different expression levels of metabolites between Control and Sh*OPA1* (two-way ANOVA, n=3). (D) Schematic of glycolysis and TCA cycle process. Green arrows represent down-regulated metabolites. Red arrows represent up-regulated metabolites. (E) Knockdown of OPA1 decreased the aerobic respiration rates as indicated by the OCR. (F) Basal respiration, Proton Leak, ATP production and maximal respiration was lower in *OPA1* knockdown NCIH1299 cells. For F, the bars represent mean ± SEM. The statistical analysis was carried out using t-test, denotes $P < 0.01$.

Figure 4. *OPA1* modulates immune evasion of tumor epithelial to CD8$^+$ T cells.

(A)GO analysis of downregulated gene in OPA1 overexpressed LUAD cells, red represent biological process, green represent cell component, blue represent molecular function. (B) GSEA analysis for immune response pathway. (C) mRNA expression of immune response related gene in control and OPA1 knocked down cells. (D and E) Distribution (D) and proportion (E) of OPA1 gene expression in different cell types; (F) The expression proportion of MKI67 gene in different cell types of OPA1$^+$ and OPA1$^-$. (G) GO biological process enrichment analysis within the complete set of differentially expressed genes in OPA1$^+$ and OPA1$^-$ tumor tissues. (H and I) Capacity for intercellular communication between tumor epithelial cells and other cells. Width of lines indicates the strength of interactions between the indicated cell types.

Figure 5. Knockdown of *OPA1* increases apoptosis in NCI-H1299 cells.

(A&B) Representative confocal images of mitochondria with TMRM staining in Control and Sh*OPA1* cells. Scale bars, 20μm (C) Western blotting detected the expression of and OPA1 and cytochrome c in Control and Sh*OPA1* cells. GAPDH used as a loading control. (D) Flow cytometry analysis of cell cycle status in Control and Sh*OPA1* cells. Statistical results are present on right, indicating knockdown-*OPA1* cells was significantly stalled at the G1/G0 phase. (E) RT-PCR detected the mRNA expression levels of *CDK1*, *CDC25a* and *CCND1* in Control and Sh*OPA1* cells, and *GAPDH* gene used as a control. (F) Increased apoptosis of NCI-H1299 cells with down-regulated *OPA1* in the representative scatter plots of flow cytometry and quantification analysis. For

A to E, n=3 and the bars represent mean ± SEM. The statistical analysis was carried out using t-test, * denotes $P < 0.05$, ** denotes $P < 0.01$.

Figure 6. *OPA1* modulates LUAD proliferation and migration.

(A) mRNA expression levels of *OPA1* in Control and Sh*OPA1* NCI-A549 cells. (B) Cell proliferation was measured by CCK8 assay in Control and Sh*OPA1* NCI-A549 cells. (C) Colonies were counted in Control and Sh*OPA1* NCI-A549 cells, statistical results are present on right. (D) Representative images of transwell assays (migration) in Control and Sh*OPA1* NCI-A549 cells. Statistical results are present on right. Scale bars, 100μm. (E) mRNA expression levels of OPA1 in Control and Sh*OPA1* NCI-H1299 cells. (F) Cell proliferation was measured by CCK8 assay in Control and Sh*OPA1* NCI-H1299 cells. (G) Colonies were counted in Control and Sh*OPA1* NCI-H1299 cells, statistical results are present on right. (H) Representative images of transwell assays (migration) in Control and Sh*OPA1* NCI-H1299 cells. (I) mRNA levels of *OPA1* after 48h when transfected with *OPA1* overexpression constructs and empty vectors in NCI-A549 cells. (J) Cell proliferation was measured by CCK8 assay in *OPA1* overexpression and control NCI-A549 cells. (K) Colonies were counted in *OPA1* overexpression and control NCI-A549 cells. (L) Representative images of transwell assays (migration) after 48h when transfected with *OPA1* overexpression constructs and empty vectors in NCI-A549 cells. Scale bars, 500μm. Statistical results are present on right. Scale bars, 100μm. For A to H, n=3 and the bars represent mean ± SEM. The statistical analysis was carried out using t-test, ns denotes no significance, * denotes $P < 0.05$, ** denotes $P < 0.01$.

Figure 7. *OPA1* supports mitochondrial fusion and respiratory function in lung adenocarcinoma.

In tumor cells, the high expression of *OPA1* promoted mitochondrial fusion and maintain a healthy mitochondrial network at the inner membrane. The enough production of ATP facilitated the proliferation of tumor cells. In Sh*OPA1* cells, the loss of *OPA1* induced structural and functional abnormalities of the mitochondria and contributed to the apoptosis.

Figure 1

Figure 1. The high expression and function of *OPA1* in LUAD.

(A) Mitochondrial dynamics-related genes (*MFN1/2*, *OPA1* and *DNM1L*) are highly expressed in tumor tissues based on TCGA database . (B) Schematic diagram showing somatic alterations in the genes identified in NSCLC. Amplification (red) was displayed. (C-D) Copy number alterations of OPA1 and MFN1 in NSCLC samples from TCGA data (C) and a box plot showing the association between mRNA levels and gene amplification or deletion (D). (E) Immunohistochemical examination of OPA1 expression in adjacent (N=55) and tumor (N=55) tissues, H-score: the depth and quantity of positivity scored by Quant Center, an analysis software matching with 3D scanner. H-score detected by image j and used to evaluate the protein expression of OPA1. (F) The correlation between the expression of OPA1, MFN1 and survival of LUAD patients. For D to F, data are expressed as the means ± SEM. The statistical analysis was carried out using t-test.

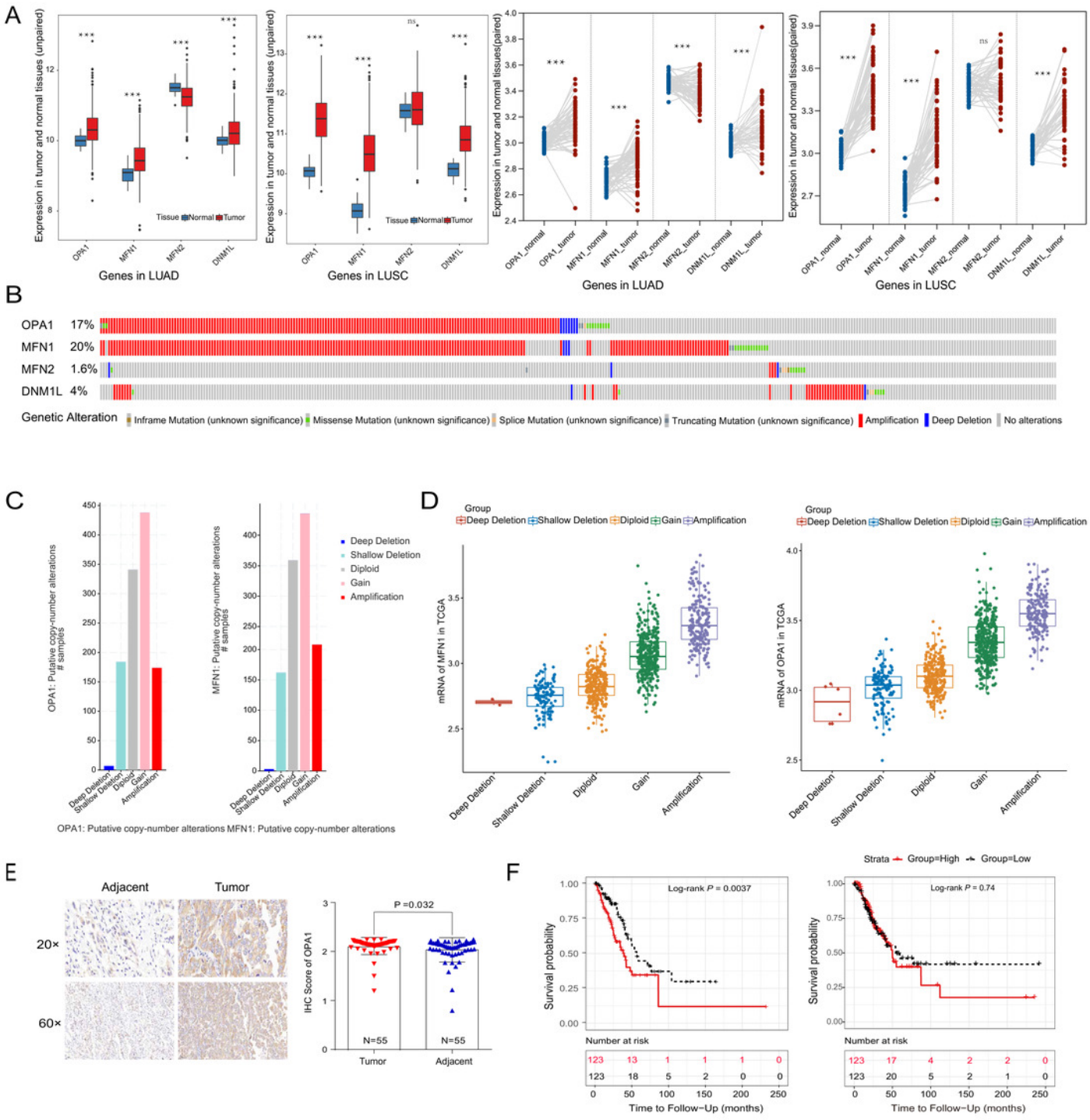
A
Expression in tumor and normal tissues (unpaired)
Tissue Normal Tumor
OPA1
MFN1
MFN2
DNM1L
Genes in LUAD
Genes in LUSC
Expression in tumor and normal tissues(paired)
OPA1_normal
OPA1_tumor
MFN1_normal
MFN1_tumor
MFN2_normal
MFN2_tumor
DNM1L_normal
DNM1L_tumor
B
OPA1 17%
MFN1 20%
MFN2 1.6%
DNM1L 4%
Genetic Alteration
Inframe Mutation (unknown significance)
Missense Mutation (unknown significance)
Splice Mutation (unknown significance)
Truncating Mutation (unknown significance)
Amplification
Deep Deletion
No alterations
C
OPA1: Putative copy-number alterations # samples
MFN1: Putative copy-number alterations # samples
Deep Deletion
Shallow Deletion
Diploid
Gain
Amplification
OPA1: Putative copy-number alterations MFN1: Putative copy-number alterations
D
Group
Deep Deletion
Shallow Deletion
Diploid
Gain
Amplification
mRNA of MFN1 in TCGA
mRNA of OPA1 in TCGA
E
Adjacent
Tumor
20×
60×
IHC Score of OPA1
P =0.032
N=55
N=55
Tumor
Adjacent
F
Strata
Group=High
Group=Low
Survival probability
Log-rank P = 0.0037
Log-rank P = 0.74
Number at risk
Time to Follow-Up (months)

Figure 2

Figure 2. Loss of *OPA1* induced mitochondrial dysfunction and decreased ATP production.

(A) Volcano plot of statistical significance ($P<0.05$) against fold change (ratio of Sh*OPA1*/Control group), demonstrating the most significantly differentially expressed genes by genome-wide transcriptomic analysis between Control and Sh*OPA1* NCI-H1299 cells. (B) Heat map of color-coded expression levels of differentially expressed genes (two-way ANOVA (n=3)). (C) GO pathway enrichment analysis within the complete set of differentially expressed genes. (D, E) GSEA enrichment plots showing that loss of *OPA1* results in the dysfunction of MITOCHONDRIA_GENE_MODULE and ATP_METABOLIC_PROCESS gene set. (F) Transmission electron microscopy was used to observe mitochondrial morphology and combined with Image J measurement to analyze the changes in the area and number in Control and Sh*OPA1* NCI-H1299 cells. Scale bars, 500nm. (G) ATP production was detected in Control and Sh*OPA1* cells. Abbreviations: CC, Cellular Component; BP, Biological Process; MF, Molecular Function. For A to G, n=3 and the bars represent mean ± SEM. The statistical analysis was carried out using t-test, NS denotes no significant, ** denotes $P < 0.01$.

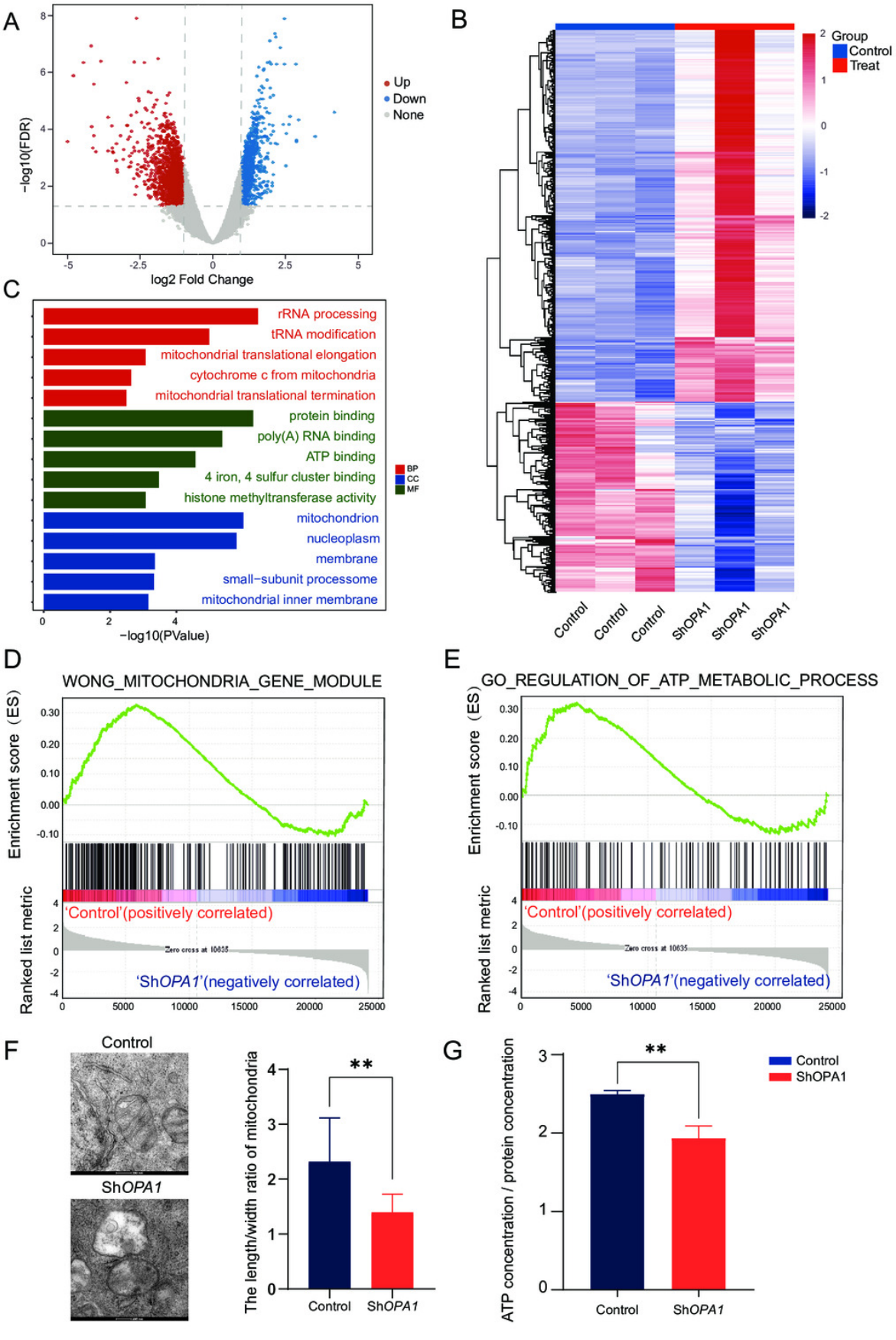
A
Up
Down
None
−log10(FDR)
log2 Fold Change
B
Group
Control
Treat
Control
Control
Control
ShOPA1
ShOPA1
ShOPA1
C
rRNA processing
tRNA modification
mitochondrial translational elongation
cytochrome c from mitochondria
mitochondrial translational termination
protein binding
poly(A) RNA binding
ATP binding
4 iron, 4 sulfur cluster binding
histone methyltransferase activity
mitochondrion
nucleoplasm
membrane
small−subunit processome
mitochondrial inner membrane
BP
CC
MF
−log10(PValue)
D
WONG_MITOCHONDRIA_GENE_MODULE
Enrichment score (ES)
Ranked list metric
'Control'(positively correlated)
'ShOPA1'(negatively correlated)
E
GO_REGULATION_OF_ATP_METABOLIC_PROCESS
Enrichment score (ES)
Ranked list metric
'Control'(positively correlated)
'ShOPA1'(negatively correlated)
F
Control
ShOPA1
The length/width ratio of mitochondria
Control
ShOPA1
G
ATP concentration / protein concentration
Control
ShOPA1
Control
ShOPA1

Figure 3

Figure 3. Knockdown of *OPA1* decreased the metabolic efficiency in NCI-H1299 cells.

(A) Metabolites were analyzed by PLS-DA. Each principal component is labeled with the corresponding percent values. (B) Variable importance on projection (VIP) represented the importance of the substance in the PLS-DA model. (C) Heatmap analysis of different expression levels of metabolites between Control and Sh*OPA1* (two-way ANOVA, n=3). (D) Schematic of glycolysis and TCA cycle process. Green arrows represent down-regulated metabolites. Red arrows represent up-regulated metabolites. (E) Knockdown of OPA1 decreased the aerobic respiration rates as indicated by the OCR. (F) Basal respiration, Proton Leak, ATP production and maximal respiration was lower in *OPA1* knockdown NCIH1299 cells. For A-F, n=3 and the bars represent mean ± SEM. The statistical analysis was carried out using t-test, denotes $P < 0.01$.

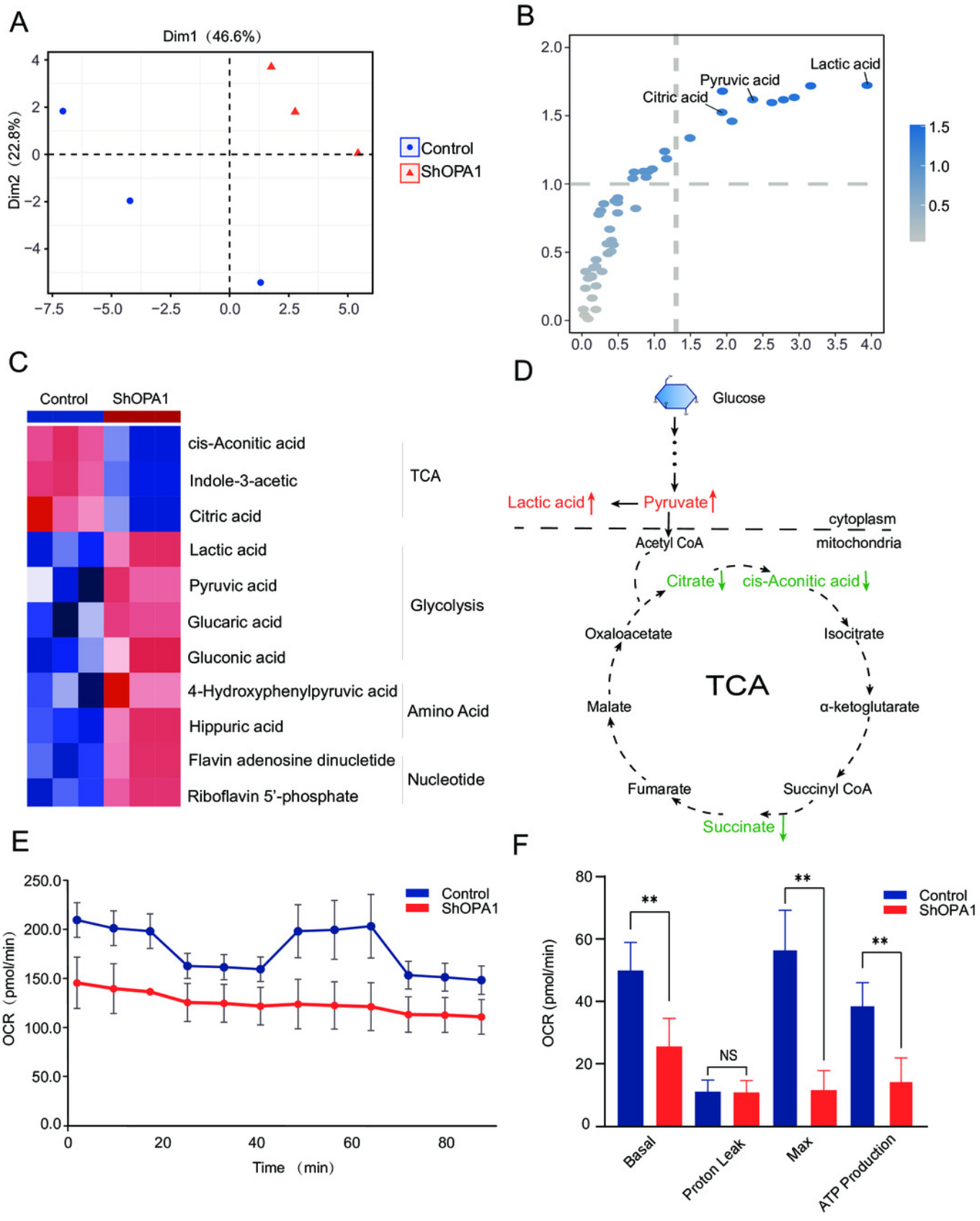
A
Dim1 (46.6%)
Dim2 (22.8%)
Control
ShOPA1
B
Lactic acid
Pyruvic acid
Citric acid
C
Control
ShOPA1
cis-Aconitic acid
Indole-3-acetic
Citric acid
Lactic acid
Pyruvic acid
Glucaric acid
Gluconic acid
4-Hydroxyphenylpyruvic acid
Hippuric acid
Flavin adenosine dinucletide
Riboflavin 5'-phosphate
TCA
Glycolysis
Amino Acid
Nucleotide
D
Glucose
Lactic acid
Pyruvate
cytoplasm
mitochondria
Acetyl CoA
Citrate
cis-Aconitic acid
Oxaloacetate
Isocitrate
TCA
Malate
α-ketoglutarate
Fumarate
Succinyl CoA
Succinate
E
OCR (pmol/min)
Time (min)
Control
ShOPA1
F
OCR (pmol/min)
Control
ShOPA1
NS
Basal
Proton Leak
Max
ATP Production

Figure 4

Figure 4. *OPA1* modulates immune evasion of tumor epithelial to $CD8^+$ T cells.

(A)GO analysis of downregulated gene in OPA1 overexpressed LUAD cells, red represent biological process, green represent cell component, blue represent molecular function. (B) GSEA analysis for immune response pathway. (C) mRNA expression of immune response related gene in control and OPA1 knocked down cells. (D and E) Distribution (D) and proportion (E) of OPA1 gene expression in different cell types; (F) The expression proportion of MKI67 gene in different cell types of $OPA1^+$ and $OPA1^-$. (G) GO biological process enrichment analysis within the complete set of differentially expressed genes in $OPA1^+$ and $OPA1^-$ tumor tissues. (H and I) Capacity for intercellular communication between tumor epithelial cells and other cells. Width of lines indicates the strength of interactions between the indicated cell types.

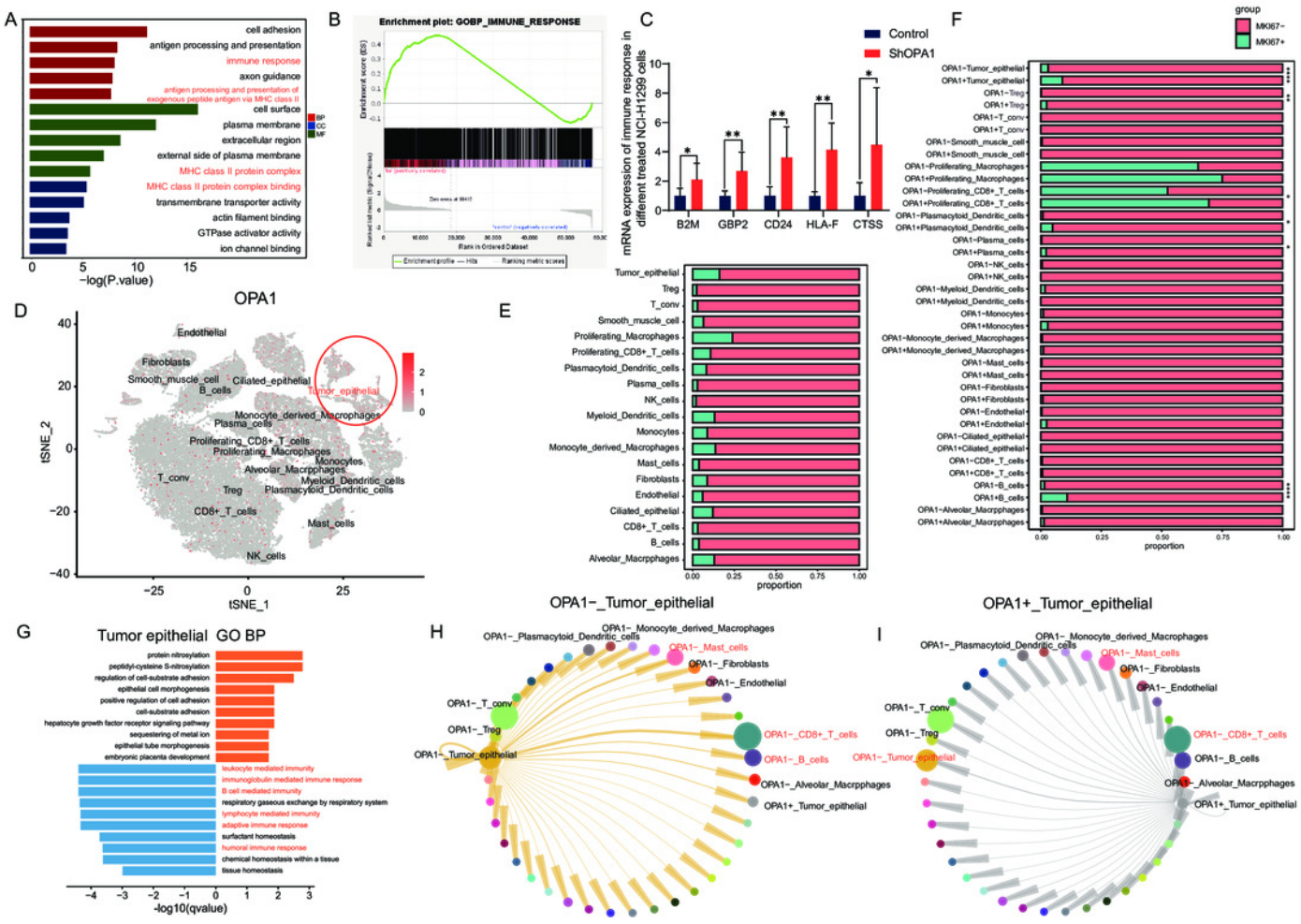
A
cell adhesion
antigen processing and presentation
immune response
axon guidance
antigen processing and presentation of exogenous peptide antigen via MHC class II
cell surface
plasma membrane
extracellular region
external side of plasma membrane
MHC class II protein complex
MHC class II protein complex binding
transmembrane transporter activity
actin filament binding
GTPase activator activity
ion channel binding
BP
CC
MF
−log(P.value)
B
Enrichment plot: GOBP_IMMUNE_RESPONSE
C
Control
ShOPA1
mRNA expression of immune response in different treated NCI-H1299 cells
B2M
GBP2
CD24
HLA-F
CTSS
D
OPA1
Endothelial
Fibroblasts
Smooth_muscle_cell
Ciliated_epithelial
B_cells
Tumor_epithelial
Monocyte_derived_Macrophages
Plasma_cells
Proliferating_CD8+_T_cells
Proliferating_Macrophages
Monocytes
Alveolar_Macrpphages
T_conv
Myeloid_Dendritic_cells
Treg
Plasmacytoid_Dendritic_cells
CD8+_T_cells
Mast_cells
NK_cells
tSNE_1
tSNE_2
E
proportion
F
group
MKI67−
MKI67+
proportion
G
Tumor epithelial GO BP
protein nitrosylation
peptidyl-cysteine S-nitrosylation
regulation of cell-substrate adhesion
epithelial cell morphogenesis
positive regulation of cell adhesion
cell-substrate adhesion
hepatocyte growth factor receptor signaling pathway
sequestering of metal ion
epithelial tube morphogenesis
embryonic placenta development
leukocyte mediated immunity
immunoglobulin mediated immune response
B cell mediated immunity
respiratory gaseous exchange by respiratory system
lymphocyte mediated immunity
adaptive immune response
surfactant homeostasis
humoral immune response
chemical homeostasis within a tissue
tissue homeostasis
-log10(qvalue)
H
OPA1−_Tumor_epithelial
OPA1−_Monocyte_derived_Macrophages
OPA1−_Plasmacytoid_Dendritic_cells
OPA1−_Mast_cells
OPA1−_Fibroblasts
OPA1−_Endothelial
OPA1−_T_conv
OPA1−_Treg
OPA1−_CD8+_T_cells
OPA1−_B_cells
OPA1−_Alveolar_Macrpphages
OPA1+_Tumor_epithelial
I
OPA1+_Tumor_epithelial
OPA1−_Monocyte_derived_Macrophages
OPA1−_Plasmacytoid_Dendritic_cells
OPA1−_Mast_cells
OPA1−_Fibroblasts
OPA1−_Endothelial
OPA1−_T_conv
OPA1−_Treg
OPA1−_Tumor_epithelial
OPA1−_CD8+_T_cells
OPA1−_B_cells
OPA1−_Alveolar_Macrpphages
OPA1+_Tumor_epithelial

Figure 5

Figure 5. Knockdown of *OPA1* increases apoptosis in NCI-H1299 cells.

(A&B) Representative confocal images of mitochondria with TMRM staining in Control and Sh*OPA1* cells. Scale bars, 20μm (C) Western blotting detected the expression of cytochrome c in Control and Sh*OPA1* cells. GAPDH used as a loading control. (D) Flow cytometry analysis of cell cycle status in Control and Sh*OPA1* cells. Statistical results are present on right, indicating knockdown-*OPA1* cells was significantly stalled at the G1/G0 phase. (E) RT-PCR detected the mRNA expression levels of *CDK1*, *CDC25a* and *CCND1* in Control and Sh*OPA1* cells, and *GAPDH* gene used as a control. (F) Increased apoptosis of NCI-H1299 cells with down-regulated *OPA1* in the representative scatter plots of flow cytometry and quantification analysis. For A to E, n=3 and the bars represent mean ± SEM. The statistical analysis was carried out using t-test, * denotes $P < 0.05$, ** denotes $P < 0.01$.

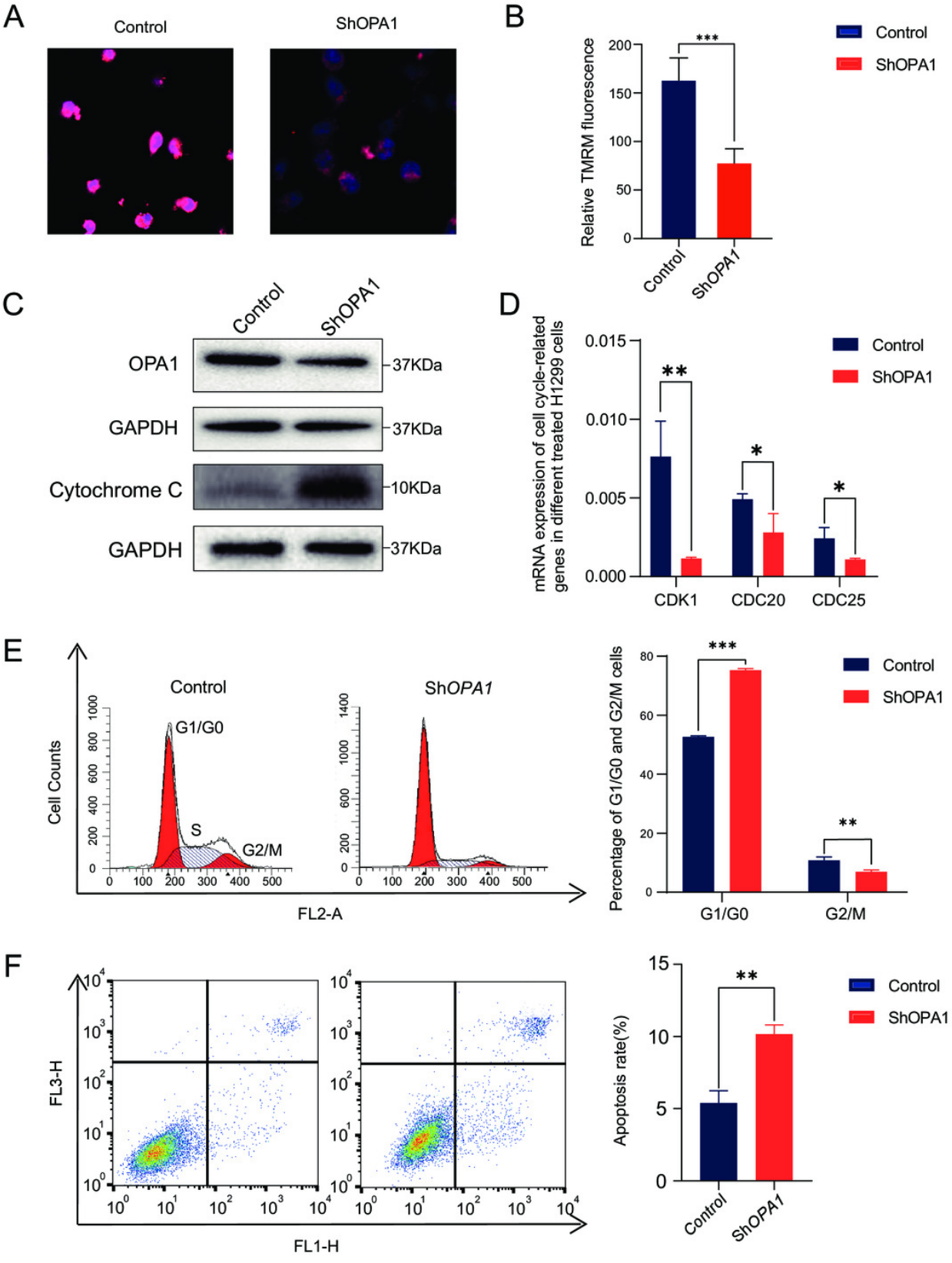
A
Control
ShOPA1
B
Relative TMRM fluorescence
***
Control
ShOPA1
C
Control
ShOPA1
OPA1
37KDa
GAPDH
37KDa
Cytochrome C
10KDa
GAPDH
37KDa
D
mRNA expression of cell cycle-related genes in different treated H1299 cells
**
*
*
CDK1
CDC20
CDC25
E
Control
ShOPA1
Cell Counts
G1/G0
S
G2/M
FL2-A
Percentage of G1/G0 and G2/M cells
***
**
G1/G0
G2/M
F
FL3-H
FL1-H
Apoptosis rate(%)
**

Figure 6

Figure 6. *OPA1* modulates LUAD proliferation and migration.

(A) mRNA expression levels of *OPA1* in Control and Sh*OPA1* NCI-A549 cells. (B) Cell proliferation was measured by CCK8 assay in Control and Sh*OPA1* NCI-A549 cells. (C) Colonies were counted in Control and Sh*OPA1* NCI-A549 cells, statistical results are present on right. (D) Representative images of transwell assays (migration) in Control and Sh*OPA1* NCI-A549 cells. Statistical results are present on right. Scale bars, 100μm. (E) mRNA expression levels of OPA1 in Control and Sh*OPA1* NCI-H1299 cells. (F) Cell proliferation was measured by CCK8 assay in Control and Sh*OPA1* NCI-H1299 cells. (G) Colonies were counted in Control and Sh*OPA1* NCI-H1299 cells, statistical results are present on right. (H) Representative images of transwell assays (migration) in Control and Sh*OPA1* NCI-H1299 cells.(I) mRNA levels of *OPA1* after 48h when transfected with *OPA1* overexpression constructs and empty vectors in NCI-A549 cells. (J) Cell proliferation was measured by CCK8 assay in *OPA1* overexpression and control NCI-A549 cells. (K) Colonies were counted in *OPA1*overexpression and control NCI-A549 cells. (L) Representative images of transwell assays (migration) after 48h when transfected with *OPA1* overexpression constructs and empty vectors in NCI-A549 cells. Scale bars, 500μm. Statistical results are present on right. Scale bars, 100μm. For A to H, n=3 and the bars represent mean ± SEM. The statistical analysis was carried out using t-test, ns denotes no significance, * denotes $P < 0.05$, ** denotes $P < 0.01$.

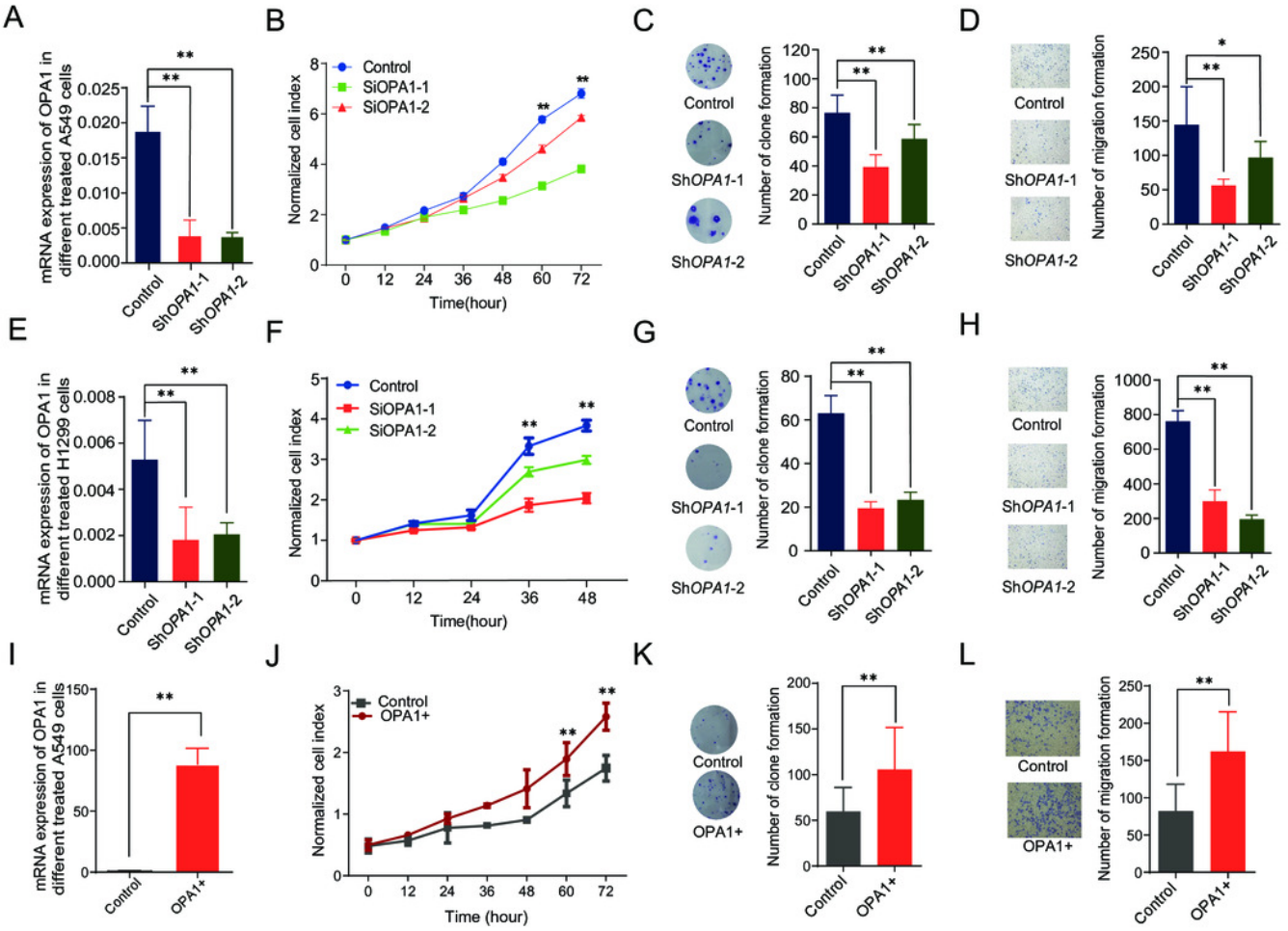
A
mRNA expression of OPA1 in different treated A549 cells
Control
ShOPA1-1
ShOPA1-2
B
Normalized cell index
Time(hour)
Control
SiOPA1-1
SiOPA1-2
C
Number of clone formation
D
Number of migration formation
E
mRNA expression of OPA1 in different treated H1299 cells
F
Normalized cell index
Time(hour)
G
Number of clone formation
H
Number of migration formation
I
mRNA expression of OPA1 in different treated A549 cells
OPA1+
J
Normalized cell index
Time (hour)
K
Number of clone formation
L
Number of migration formation

Figure 7

Figure 7. *OPA1* supports mitochondrial fusion and respiratory function in lung adenocarcinoma.

In tumor cells, the high expression of *OPA1* promoted mitochondrial fusion and maintain a healthy mitochondrial network at the inner membrane. The enough production of ATP facilitated the proliferation of tumor cells. In Sh*OPA1* cells, the loss of *OPA1* induced structural and functional abnormalities of the mitochondria and contributed to the apoptosis.

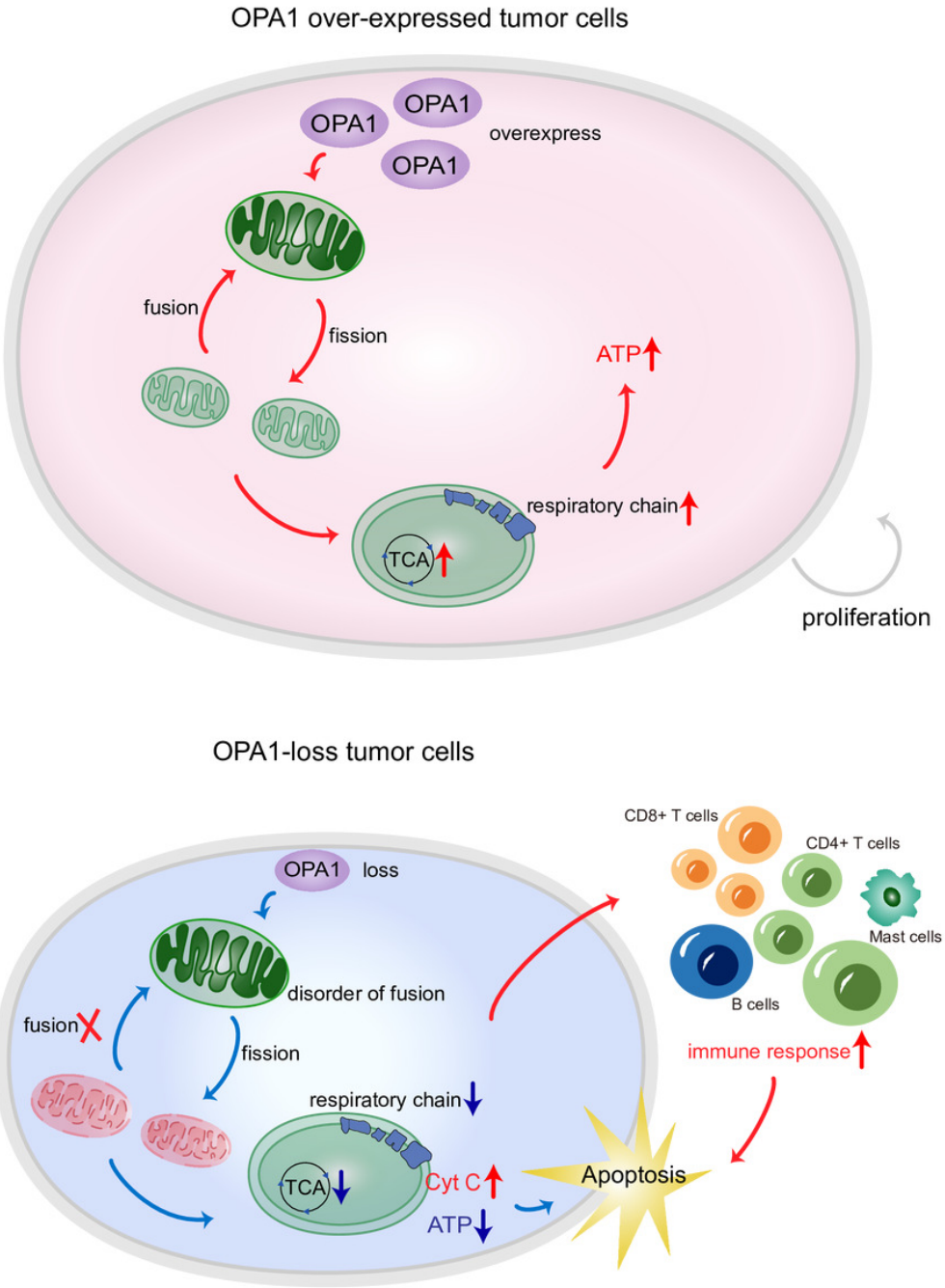
OPA1 over-expressed tumor cells
OPA1
OPA1
OPA1
overexpress
fusion
fission
ATP
respiratory chain
TCA
proliferation
OPA1-loss tumor cells
OPA1 loss
disorder of fusion
fusion
fission
respiratory chain
TCA
Cyt C
ATP
Apoptosis
CD8+ T cells
CD4+ T cells
Mast cells
B cells
immune response